Research Article | Vol. 31, No. 12 / 5 Jun 2023 / Optics Express 20377

Optics EXPRESS

KGW and YVO_4: two excellent nonlinear materials for high repetition rate infrared supercontinuum generation

VAIDA MARČIULIONYTĖ, KAWTHAR REGGUI, GINTARAS TAMOŠAUSKAS, AND AUDRIUS DUBIETIS*

Laser Research Center, Vilnius University, Saulėtekio Avenue 10, LT- 10223 Vilnius, Lithuania
**audrius.dubietis@ff.vu.lt*

Abstract: We present an experimental investigation of supercontinuum generation in potassium gadolinium tungstate (KGW) and yttrium vanadate (YVO_4) crystals pumped with 210 fs, 1030 nm pulses from an amplified Yb:KGW laser operating at 2 MHz repetition rate. We demonstrate that compared to commonly used sapphire and YAG, these materials possess considerably lower supercontinuum generation thresholds, produce remarkable red-shifted spectral broadenings (up to 1700 nm in YVO_4 and up to 1900 nm in KGW) and exhibit less bulk heating due to energy deposition during filamentation process. Moreover, durable damage-free performance was observed without any translation of the sample, suggesting that KGW and YVO_4 are excellent nonlinear materials for high repetition rate supercontinuum generation in the near and short-wave infrared spectral range.

1. Introduction

Supercontinuum (SC) generation via filamentation of ultrashort laser pulses in transparent bulk solid-state materials represents a simple, robust, and well-established technique for the production of broadband radiation with a high degree of coherence that ensures excellent compressibility and focusability of pulses and beams carrying more than octave-spanning spectra [1,2]. For these reasons SC generation emerges as the only reliable seed source for ultrafast optical parametric amplifiers (OPAs) [3–5], offering high energy stability, excellent pulse compressibility along with preservation of stable carrier-envelope phase, and low time jitter between the pump and seed pulses [6]. SC generation is also widely exploited in table-top optical parametric chirped pulse amplifiers, either serving as a suitable seed directly, see e.g., [7–12] or being employed in the intermediate stages of more complex broadband seed production setups, see [13] for a review.

The advent of ultrafast high repetition rate solid-state lasers based on Yb-doped lasing media prompted the development of OPAs operating at repetition rates from tens of kHz to a few MHz. The second and third harmonics-pumped OPAs are seeded by visible (blue-shifted) portion of the SC [14–19], while fundamental harmonic-pumped OPAs use the near and short-wave infrared (red-shifted) portions of the SC spectrum [20–24] that is typically generated by filamentation of fundamental harmonic pulses in either sapphire or YAG crystals, which are the most reliable nonlinear materials for this purpose [25]. The vast majority of SC generation setups with Yb lasers employ YAG, which, compared to sapphire, has larger nonlinearity and exhibits superior resistance to optical degradation at high laser pulse repetition rates, demonstrating robust performance even with tightly focused pump beams [26].

However, the energy trade-off between the pump channels of SC generation and subsequent OPA stage(s) becomes very important for the state-of-the-art laser systems operating at MHz repetition rates, and demands the nonlinear materials with lower SC generation thresholds than conventional materials such as sapphire and YAG currently offer. To this end, narrow bandgap dielectric crystals, such as potassium gadolinium tungstate ($KGd(WO_4)_2$, KGW) and yttrium

#489474 https://doi.org/10.1364/OE.489474
Journal © 2023 Received 8 Mar 2023; revised 19 May 2023; accepted 23 May 2023; published 1 Jun 2023

Optics EXPRESS

vanadate (YVO_4), owing to their large values of nonlinear refractive indexes [27] emerge as potentially attractive candidates for this purpose. Although these materials produce only modest spectral broadenings on the short-wavelength side [25], more recent experiments with 1.03 and 1.55 μm pumping demonstrate their capability to produce reasonable red-shifted spectral broadenings and a potential to operate at high repetition rates [28,29].

In this work, we carried out a comparative experimental study of SC generation in sapphire, YAG, KGW and YVO_4 crystals at a laser pulse repetition rate of 2 MHz. The measurements of SC generation thresholds, dynamics of spectral broadening, nonlinear loses and associated bulk heating demonstrate that compared to conventional nonlinear materials, such as sapphire and YAG, KGW and YVO_4 offer a number of important advantages for high repetition rate SC generation in the near and short-wave infrared spectral range.

2. Materials and methods

The experiments were performed with an amplified Yb:KGW laser (Carbide, Light Conversion Ltd.), which operated at 2 MHz repetition rate and provided 210 fs pulses with a central wavelength of 1030 nm. The comparative study of SC generation was carried out in uncoated and undoped samples of sapphire, YAG, KGW and YVO_4, whose relevant optical properties are listed in Table 1. Sapphire and YAG samples were of 6 mm length, while the available lengths of KGW (b-cut, EKSMA Optics) and YVO_4 (Optogama) samples were 10 mm. However, such a length difference had no influence on beam filamentation and SC generation dynamics, since relatively tight focusing of the pump beam was used.

Table 1. Relevant optical properties of sapphire, YAG, KGW and YVO_4. E_g is the energy bandgap, n_0 and n_2 are linear and nonlinear refractive indexes, respectively, and P_{cr} is the critical power for self-focusing calculated for the laser wavelength of 1030 nm.

Material	E_g	n_0	n_2	P_{cr}	Reference
	eV		10^{-16} cm^2/W	MW	
Sapphire	9.0	1.76	2.75	3.25	[30]
YAG	6.5	1.83	6.2	1.39	[31]
KGW	4.25	2.01	11	0.71	[27]
YVO_4	3.69	2.17	15	0.48	[27]

The experimental layout is depicted in Fig. 1. The laser beam with a diameter of 4.3 mm (at the $1/e^2$ intensity level) was focused onto the front face of the nonlinear crystal sample (S) with a fused silica lens L (f = +150 mm), which is equivalent to the numerical aperture (NA) of 0.014. Such focusing geometry was considered as optimal, since although focusing of the pump beam inside the sample may result in somewhat reduced threshold energy for SC generation, but on the other hand, increases the risk of multipulse damage due to higher intensity inside the material. On the contrary, focusing of a diverging pump beam yields an increase of the threshold energy for SC generation. The samples were kept in a stationary position during the measurements. The dynamics of spectral broadening was measured by varying the input pulse energy with an attenuator consisting of the half-wave plate (HWP) and thin-film polarizer (P). The spectral measurements were performed using two spectrometers: NIR-SWIR spectrometer (NIRQuest-512, the detection range 900-2100 nm, SP1) and UV-NIR spectrometer (AvaSpec-3648, the detection range 200-1100 nm, SP2) to measure the red-shifted and the blue-shifted parts of the SC spectrum, respectively. An achromatic lens (AL, f = +75 mm) before the NIR-SWIR spectrometer was used for a better collection of the infrared part of SC spectrum. Both spectrometers were operated simultaneously, measuring axial portions of the output radiation reflected from separate fused silica wedges (W1, W2). In order to increase the

Optics EXPRESS

dynamic range of spectral measurements, the most intense part of the SC radiation around the pump wavelength was attenuated using appropriate long-pass (F1) and short-pass (F2) filters. The measured spectra thereafter were corrected accounting for the filter transmission function and the sensitivity function of the spectrometer.

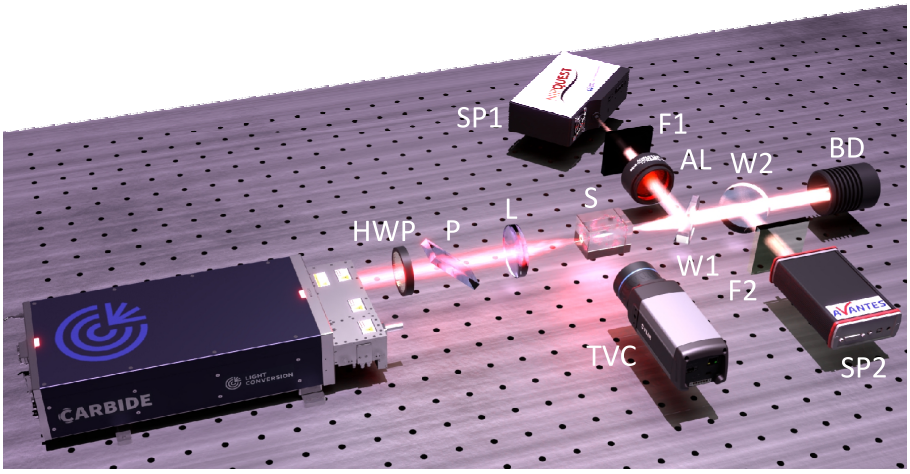

Fig. 1. The experimental layout. HWP, half-wave plate; P, thin-film polarizer; L, focusing lens; S, nonlinear crystal sample; W1, W2, fused silica wedges; F1, long-pass filter; F2, short-pass filter; AL, achromatic lens; SP1, NIR-SWIR spectrometer; SP2, UV-NIR spectrometer; TVC, thermal vision camera; BD, beam dump.

For a more detailed study of crystal performance, along with spectral measurements, we performed the measurements of nonlinear transmission and bulk heating of the tested samples. The sample transmittance as a function of the input pulse energy was measured after the removal of wedges W1 and W2 and using a thermal energy meter (Ophir 3A-PF-12), which replaced the beam dump (BD) that was used in the case of spectral measurements. The crystal temperature was monitored with a thermal vision camera (FLIR, A600-Series, TVC), which imaged the side wall of the sample, as illustrated in Fig. 1.

3. Spectral measurements

The dynamics of spectral broadening versus the input pulse energy in KGW crystal is presented in Fig. 2(a). An appreciable spectral broadening on the short wavelength side starts to be detectable with the input pulse energy of 110 nJ (after subtracting the reflection from the front face), and quickly saturates reaching a cut-off wavelength of 600 nm at the 10^{-6} intensity level on the short wavelength side with the input pulse energy of 120 nJ, which we define as the threshold energy for SC generation. However, spectral broadening on the long wavelength side shows an apparently slower character, which is attributed due to different self-steepening rates of leading and trailing sub-pulses, emerging from the pulse splitting at the nonlinear focus, that are responsible for the red-shifted and blue-shifted spectral broadenings, respectively [32]. As a result, the optimized red-shifted spectral extent (with the long-wavelength cut-off at 1900 nm) is achieved using a slightly higher input pulse energy (180 nJ, hereafter defined as the optimal energy), above which the red-shifted part of the SC spectrum still continues to broaden, but the entire SC spectrum develops strong periodic modulation. The spectral modulation is associated with filament refocusing, which leads to secondary pulse splitting, and hence to the interference between the primary and secondary split sub-pulses. Note that in the femtosecond regime, due to large group velocity mismatch, no signal with a Stokes shift due to stimulated Raman scattering

Optics EXPRESS

is detected, which is otherwise exploited for Raman frequency shifting, amplification, spectral broadening and subsequent compression of picosecond pulses [33–35].

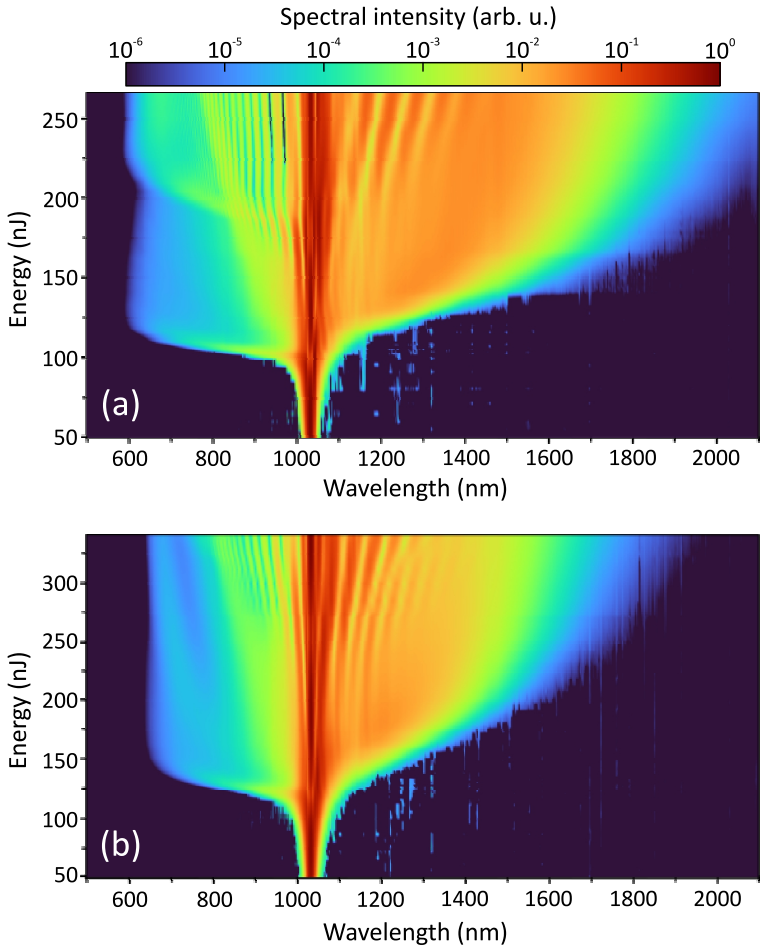

Fig. 2. The dynamics of spectral broadening versus the input pulse energy measured in (a) KGW, (b) YVO_4 crystals.

The spectral dynamics as a function of the input pulse energy in YVO_4 crystal is shown in Fig. 2(b), where we observed basically identical evolution of the SC spectrum related to general features of the filamentation process, as discussed above. However, despite a slightly larger nonlinear index of refraction, see Table 1, the SC generation threshold in YVO_4 was found somewhat higher (150 nJ) and with the optimal input pulse energy of 230 nJ the SC spectrum in YVO_4 covered the 650 – 1700 nm range.

Figure 3 compares the SC emission patterns produced in KGW and YVO_4, which were projected on the paper screen. In the case of KGW, Fig. 3(a), the bright spot in the center represents the axial portion of SC, which is surrounded by an array of colors from red inside to green outside, representing the conical emission (broadband radiation emerging at wavelength-dependent angle with respect to the pump beam). The light emission pattern produced in YVO_4 displays only deep-red conical emission at a large angle, whereas the infrared SC radiation on the propagation axis is visible as a distinct purple spot at the center due to paper luminescence, see Fig. 3(b). Interestingly, the respective crystal views shown at the bottom left corner of the

Optics EXPRESS

images, reveal huge differences in filament-induced luminescence. More specifically, only very faint filament-induced luminescence is observed in KGW, which is completely surpassed by the reflections of red color-dominated conical emission from the crystal faces. In contrast, the light filament in YVO_4 induced very strong broadband emission centered at ~ 450 nm, which was first observed with excitation with nanosecond pulses in the visible range and was attributed to transitions within the vanadate (VO_4^{3-}) group [36]. More recently, strong bluish luminescence in YVO_4 was observed with infrared continuous wave excitation [37], also noting a huge difference in luminescence intensities in YVO_4 and KGW, which is still missing a plausible explanation.

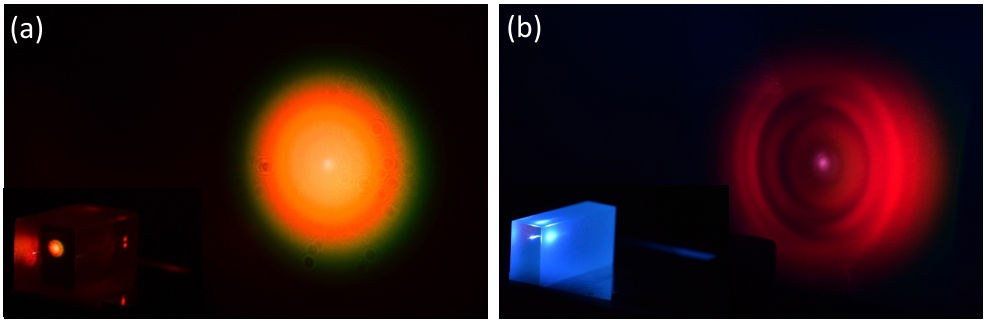

Fig. 3. SC emission patterns produced in (a) KGW, (b) YVO_4 with the optimum input pulse energies of 180 nJ and 230 nJ, respectively. Crystal views are seen at the bottom left corner of the images.

The dynamics of spectral broadening under identical focusing conditions were also measured in sapphire and YAG crystals, allowing a straightforward comparison of SC generation performances in all tested materials. The measured threshold energies for SC generation in sapphire and YAG crystals were 880 nJ and 410 nJ, respectively. A smooth SC spectrum covering the 460 – 1500 nm range was produced in sapphire with optimal input pulse energy of 1.1 μJ, while the SC spectrum in the range of 490 – 1500 nm was generated in YAG with optimal input pulse energy of 730 nJ. Note that the relatively tight focusing condition (NA=0.014) used in the present experiment did not allow to achieve an improved spectral broadening toward the long-wavelength side in both materials [25,32].

Figure 4 presents the relevant characteristics of SC radiation, which are important from a practical point of view. Figure 4(a) shows the comparison of SC spectra in sapphire, YAG, KGW and YVO_4 in terms of spectral energy density. Figure 4(b) depicts the long wavelength parts of the SC spectra in KGW and YVO_4, measured with optimal input pulse energies (180 nJ and 230 nJ, respectively) on a linear scale. Strong spectral modulations are present at the vicinity of the pump wavelength (up to ~ 1200 nm), whereas the major portions of the SC spectra are smooth and modulation-free. The high spatial quality of the SC beam is attested by Figs. 4(c) and 4(d), which display the SC beam profiles in KGW and YVO_4, respectively, within the 1200 – 1400 nm spectral window selected by appropriate filtering and measured with InGaAs camera (C12741-03, Hamamatsu) located at 10 cm distance from the sample exit face.

To briefly summarize the spectral measurements in all tested materials, the established SC generation thresholds in KGW and YVO_4 were considerably lower than in YAG (~ 3 times) and sapphire (5 to 7 times), in fair agreement with the values of critical power for self-focusing provided in Table 1. However, it is interesting to mention that KGW crystal has lower SC generation threshold than YVO_4, although the opposite could be expected. Moreover, the attained blue-shifts of the SC spectra nicely confirm the general and well-established bandgap dependence [38], see also [39] for the most recent updates. In that regard, since both KGW and YVO_4 produce only moderate spectral blue shifts, YAG crystal remains the primary choice for what concerns

Optics EXPRESS

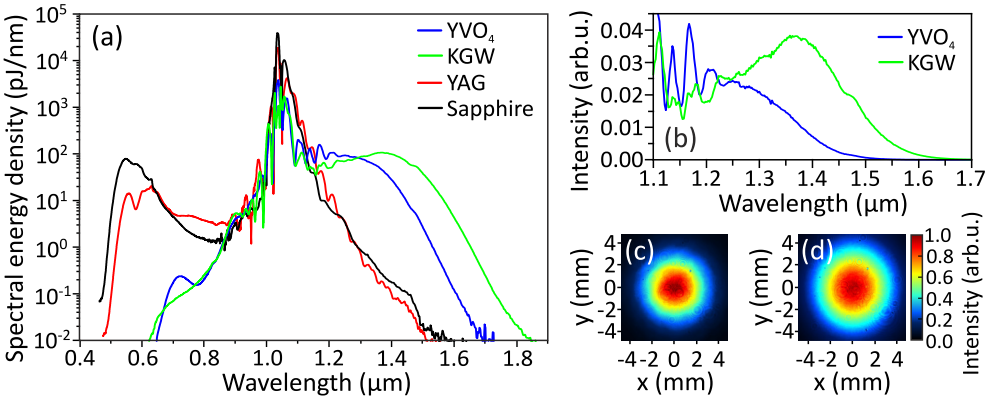

Fig. 4. (a) Comparison of SC spectra in sapphire, YAG, KGW and YVO_4 produced with optimal input pulse energies. (b) The long wavelength parts of the SC spectra in KGW and YVO_4 shown on a linear scale. The SC beam profiles in (c) KGW and (d) YVO_4 measured in the 1200 – 1400 nm spectral window.

high repetition rate SC generation in the visible range. Finally, despite relatively tight focusing of the pump beam, KGW and YVO_4 produce remarkably large spectral red-shifts, which is in contrast with modest spectral red-shifts attained in sapphire and YAG under identical focusing conditions.

4. Nonlinear transmission, bulk heating and long-term performance

Energy deposition to the transparent material via multiphoton absorption and free electron plasma absorption due to the inverse Bremsstrahlung effect, which are among the key players in the filamentation process, lead to heat accumulation at very high repetition rates [40]. This may result in gradual structural modification, or, in other words, optical degradation of the material, that in turn causes shrinking, and eventually, extinction of the SC spectrum with time. Therefore, in order to gain more insight on the crystal performance from the perspective of long-term operation, we carried out the measurements of nonlinear transmission vs the input pulse energy and measured bulk heating of all tested materials.

The measured transmissions of sapphire, YAG, KGW and YVO_4 samples as functions of the input pulse energy after subtracting Fresnel reflections from crystal input and exit faces, are presented in Fig. 5(a). The onset of nonlinear losses (the drop in transmission) is associated with an increase of the beam intensity due to self-focusing, and eventually, formation of a light filament. KGW and YVO_4 samples exhibit the largest nonlinear losses in total, which are mainly contributed by low-order (four-photon) nonlinear absorption, whereas the multiphoton absorption orders of 6 and 8 were estimated in YAG and sapphire, respectively, assuming the incident photon energy of 1.2 eV and material bandgap values, listed in Table 1. Figure 5(b) shows the calculated fractional losses, defined as $-dT/dE$, which are equivalent to nonlinear absorption rate. For a fixed propagation length (the length of the sample), the peaks of fractional losses occur when the intensity growth is the fastest, that is at the nonlinear focus of the beam. In other words, the peaks of fractional losses indicate the input pulse energy, which produces the nonlinear focus right on the exit face of the sample, and which could be regarded as a threshold energy for beam filamentation, see e.g. [41] for details.

The estimated nonlinear losses in the operating conditions at the optimal input pulse energies amounted to 34%, 44%, 35% and 43% in sapphire, YAG, KGW and YVO_4 samples, respectively. These in turn yielded the absolute values of absorbed energy of 100 nJ in YVO_4, 63 nJ in KGW,

Optics EXPRESS

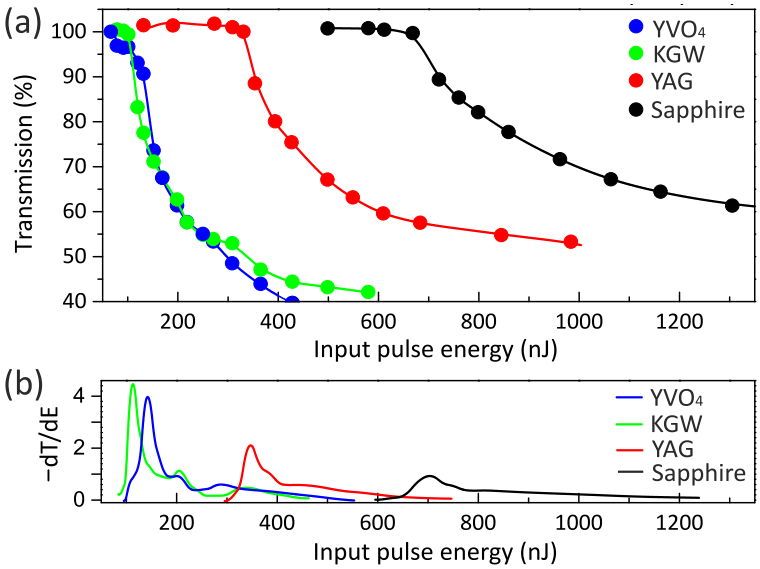

Fig. 5. (a) Nonlinear transmission of sapphire, YAG, KGW and YVO_4 samples as a function of the input pulse energy. (b) Calculated fractional losses, whose peaks indicate that the position of the nonlinear focus is located at the exit face of the sample.

320 nJ in YAG and 375 nJ in sapphire, that convert to the absorbed powers of 200 mW, 126 mW, 640 mW and 750 mW, respectively. The effect of absorbed power on bulk heating was investigated by mounting the samples on a Teflon base and performing the surface temperature measurements after 10 minutes of continuous exposure, when sample temperature has fully settled reaching a certain equilibrium value. Although the heat accumulation is apparently proportional to the absolute amount of absorbed energy and power, on the other hand, the measured surface temperatures are related also to sample dimensions and thermal conductivity of the material, so this measurement gives just a raw approximation of thermal regime, which nevertheless is important to know from a practical point of view.

Figures 6(a) and 6(b) show the thermal vision camera images of KGW (the sample dimensions $7 \times 7 \times 10$ mm^3) and YVO_4 (the sample dimensions $3 \times 5 \times 10$ mm^3) crystals operated at 2 MHz repetition rate and optimal input pulse energies of 180 nJ and 230 nJ, respectively. The measured surface temperatures of KGW and YVO_4 samples were 31° and 41°, respectively, which are well below that of e.g., sapphire sample (the sample dimensions $5 \times 5 \times 6$ mm^3), which heated up to 92° at its optimal input pulse energy of 1.1 μJ due to the largest absolute amount of absorbed power. In practice, the bulk heating could be efficiently mitigated by using an appropriate heat sink. Mounting KGW and YVO_4 samples on an aluminium heat sink resulted in a reduction of sample temperatures to 26° and 28°, respectively, see Figs. 6(c) and 6(d), which are just slightly above the ambient temperature in the lab (21°).

Finally, we examined the long-term performances of SC generation in KGW and YVO_4 crystals. In the present experiment, the crystal samples were mounted on a metal heat sink and kept in a stationary position with respect to the pump beam. KGW crystal demonstrated very stable performance without any change of the SC spectrum over 2 hours of operation, attesting no optical degradation of the material, as illustrated in Fig. 7(a). YVO_4 crystal also demonstrated an apparently stable performance, see Fig. 7(b), however, closer inspection of the spectral dynamics in time revealed a slight but gradual narrowing of the SC spectrum on the long-wavelength side by 25 nm over 2 hours of operation. A simple test by translating the sample into a fresh (unexposed)

Optics EXPRESS

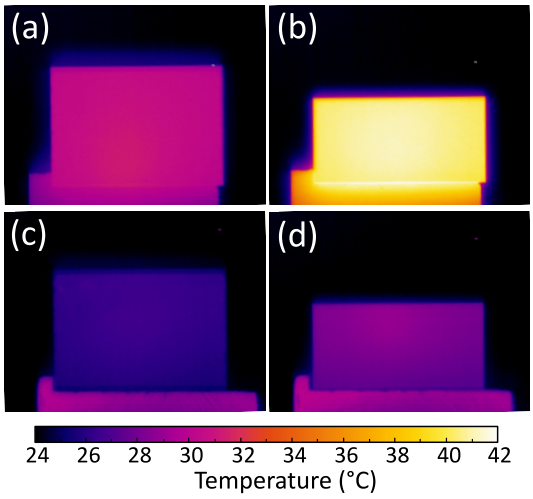

Fig. 6. Thermal vision camera images of KGW and YVO_4 samples mounted (a,b) on a Teflon base and (c,d) on an aluminium heat sink recorded after 10 min of operation at 2 MHz repetition rate with the optimal input pulse energies of 180 nJ and 230 nJ, respectively.

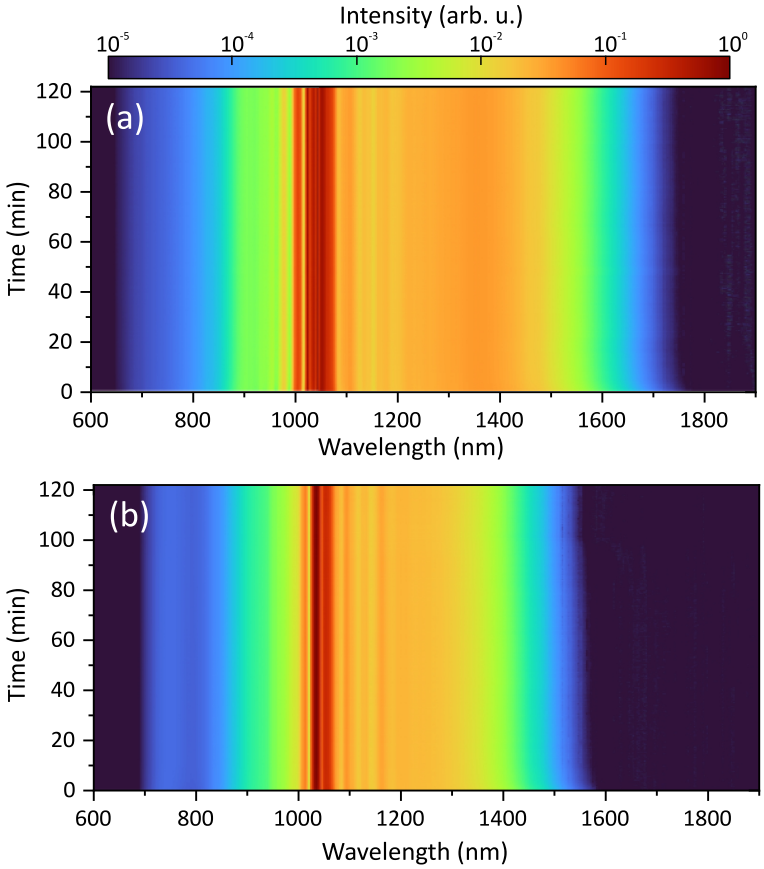

Fig. 7. Long-term dynamics of the SC spectra generated in (a) KGW

Optics EXPRESS

position showed an entirely recovered SC spectrum, so the observed spectral narrowing is indeed a signature of very slow optical degradation of YVO_4 crystal under present operating conditions. On the other hand, since the observed material degradation is very slow, it could be easily avoided by placing the crystal on the motorized translation stage.

5. Conclusions

In conclusion, we demonstrated that KGW and YVO_4 are excellent nonlinear materials for high repetition rate SC generation in the near and short-wave infrared spectral range. Both materials show durable damage-free performance at 2 MHz pulse repetition rate, negligible bulk heating and produce more than octave-wide SC spectra with remarkably large spectral red-shifts, which in combination with low filamentation and SC generation thresholds offer very suitable energy trade-off between the seed production and amplification channels for high average power ultrafast optical parametric amplifiers operating in the near- to mid-infrared spectral range. Overall, compared to YVO_4, KGW crystal demonstrated a better performance in terms of attainable spectral extent, bulk heating and optical degradation, emerging as a very useful asset for the design of high-speed spectroscopic and imaging systems which employ broadband pulses based on SC generation, see e.g. [42].

Funding. Lietuvos Mokslo Taryba (S-MIP-22-40).

Acknowledgments. The authors thank J. Banys and S. Butkus for technical support.

Disclosures. The authors declare no conflicts of interest.

Data availability. Data underlying the results presented in this paper are not publicly available at this time but may be obtained from the authors upon reasonable request.

References

1. A. Dubietis, G. Tamošauskas, R. Šuminas, V. Jukna, and A. Couairon, "Ultrafast supercontinuum generation in bulk condensed media," Lith. J. Phys. **57**(3), 113–157 (2017).
2. A. Dubietis and A. Couairon, *Ultrafast supercontinuum generation in transparent solid state media* (Springer Nature, Cham, 2019).
3. G. Cerullo and S. De Silvestri, "Ultrafast optical parametric amplifiers," Rev. Sci. Instrum. **74**(1), 1–18 (2003).
4. D. Brida, C. Manzoni, G. Cirmi, M. Marangoni, S. Bonora, P. Villoresi, S. De Silvestri, and G. Cerullo, "Few-optical-cycle pulses tunable from the visible to the mid-infrared by optical parametric amplifiers," J. Opt. **12**(1), 013001 (2010).
5. C. Manzoni and G. Cerullo, "Design criteria for ultrafast optical parametric amplifiers," J. Opt. **18**(10), 103501 (2016).
6. C. Manzoni, G. Cirmi, D. Brida, S. De Silvestri, and G. Cerullo, "Optical-parametric-generation process driven by femtosecond pulses: Timing and carrier-envelope phase properties," Phys. Rev. A **79**(3), 033818 (2009).
7. R. Riedel, A. Stephanides, M. J. Prandolini, B. Gronloh, B. Jungbluth, T. Mans, and F. Tavella, "Power scaling of supercontinuum seeded megahertz-repetition rate optical parametric chirped pulse amplifiers," Opt. Lett. **39**(6), 1422–1424 (2014).
8. M. Puppin, Y. Deng, O. Prochnow, J. Ahrens, T. Binhammer, U. Morgner, M. Krenz, M. Wolf, and R. Ernstorfer, "500 kHz OPCPA delivering tunable sub-20 fs pulses with 15 W average power based on an all-ytterbium laser," Opt. Express **23**(2), 1491–1497 (2015).
9. P. Rigaud, A. Van De Walle, M. Hanna, N. Forget, F. Guichard, Y. Zaouter, K. Guesmi, F. Druon, and P. Georges, "Supercontinuum-seeded few-cycle mid-infrared OPCPA system," Opt. Express **24**(23), 26494–26502 (2016).
10. S. Qu, H. Liang, K. Liu, X. Zou, W. Li, Q. J. Wang, and Y. Zhang, "9 μm few-cycle optical parametric chirped-pulse amplifier based on $LiGaS_2$," Opt. Lett. **44**(10), 2422–2425 (2019).
11. P. Mackonis and A. M. Rodin, "OPCPA investigation with control over the temporal shape of 1.2 ps pump pulses," Opt. Express **28**(8), 12020–12027 (2020).
12. X. Zou, W. Li, S. Qu, K. Liu, H. Li, Q. J. Wang, Y. Zhang, and H. Liang, "Flat-top pumped multi-millijoule mid-infrared parametric chirped-pulse amplifier at 10 kHz repetition rate," Laser Photonics Rev. **15**, 2000292 (2021).
13. A. Dubietis and A. Matijošius, "Table-top optical parametric chirped pulse amplifiers: past and present," Opto-Electron. Adv. **6**(3), 220046 (2023).
14. C. Schriever, S. Lochbrunner, P. Krok, and E. Riedle, "Tunable pulses from below 300 to 970 nm with durations down to 14 fs based on a 2 MHz ytterbium-doped fiber system," Opt. Lett. **33**(2), 192–194 (2008).
15. C. Homann, C. Schriever, P. Baum, and E. Riedle, "Octave wide tunable UV-pumped NOPA: pulses down to 20 fs at 0.5 MHz repetition rate," Opt. Express **16**(8), 5746–5756 (2008).

Optics EXPRESS

16. M. Emons, A. Steinmann, T. Binhammer, G. Palmer, M. Schultze, and U. Morgner, "Sub-10-fs pulses from a MHz-NOPA with pulse energies of 0.4 μJ," Opt. Express **18**(2), 1191–1196 (2010).
17. M. Bradler, C. Homann, and E. Riedle, "Mid-IR femtosecond pulse generation on the microjoule level up to 5 μm at high repetition rates," Opt. Lett. **36**(21), 4212–4214 (2011).
18. M. Bradler and E. Riedle, "Sub-20 fs μJ-energy pulses tunable down to the near-UV from a 1 MHz Yb-fiber laser system," Opt. Lett. **39**(9), 2588–2591 (2014).
19. J. Nillon, O. Crégut, C. Bressler, and S. Haacke, "Two MHz tunable non collinear optical parametric amplifiers with pulse durations down to 6 fs," Opt. Express **22**(12), 14964–14974 (2014).
20. S. B. Penwell, L. Whaley-Mayda, and A. Tokmakoff, "Single-stage MHz mid-IR OPA using $LiGaS_2$ and a fiber laser pump source," Opt. Lett. **43**(6), 1363–1366 (2018).
21. B.-H. Chen, E. Wittmann, Y. Morimoto, P. Baum, and E. Riedle, "Octave-spanning single-cycle middle-infrared generation through optical parametric amplification in $LiGaS_2$," Opt. Express **27**(15), 21306–21318 (2019).
22. Z. Heiner, V. Petrov, and M. Mero, "Efficient, sub-4-cycle, 1-μm-pumped optical parametric amplifier at 10 μm based on $BaGa_4S_7$," Opt. Lett. **45**(20), 5692–5695 (2020).
23. A. Villa, A. M. Ross, R. Gotti, M. Lamperti, F. Scotognella, G. Cerullo, and M. Marangoni, "Broadly tunable mid-infrared femtosecond pulses directly generated by an optical parametric amplifier," OSA Continuum **4**(11), 2837–2844 (2021).
24. A. Grupp, A. Budweg, M. P. Fischer, J. Allerbeck, G. Soavi, A. Leitenstorfer, and D. Brida, "Broadly tunable ultrafast pump-probe system operating at multi-kHz repetition rate," J. Opt. **20**(1), 014005 (2018).
25. M. Bradler, P. Baum, and E. Riedle, "Femtosecond continuum generation in bulk laser host materials with sub-μJ pump pulses," Appl. Phys. B **97**(3), 561–574 (2009).
26. R. Grigutis, G. Tamošauskas, V. Jukna, A. Risos, and A. Dubietis, "Supercontinuum generation and optical damage of sapphire and YAG at high repetition rates," Opt. Lett. **45**(16), 4507–4510 (2020).
27. A. G. Selivanov, I. A. Denisov, N. V. Kuleshov, and K. V. Yumashev, "Nonlinear refractive properties of Yb^{3+}-doped $KY(WO_4)_2$ and YVO_4 laser crystals," Appl. Phys. B **83**(1), 61–65 (2006).
28. K. Madeikis, P.-M. Dansette, T. Bartulevičius, L. Veselis, R. Jutas, M. Eremchev, R. Danilevičius, V. Girdauskas, and A. Michailovas, "Investigation of materials for supercontinuum generation for subsequent nonlinear parametrical and Raman amplification at 1 MHz repetition rate," Opt. Laser Technol. **143**, 107373 (2021).
29. K. R. Keller, A. Budweg, J. Allerbeck, and D. Brida, "Sub-three-cycle pulses at 2 μm from a degenerate optical parametric amplifier," Opt. Lett. **47**(7), 1594–1597 (2022).
30. B. Momgaudis, S. Guizard, A. Bilde, and A. Melninkaitis, "Nonlinear refractive index measurements using time-resolved digital holography," Opt. Lett. **43**(2), 304 (2018).
31. R. Adair, L. L. Chase, and S. A. Payne, "Nonlinear refractive index of optical crystals," Phys. Rev. B **39**(5), 3337–3350 (1989).
32. V. Jukna, J. Galinis, G. Tamošauskas, D. Majus, and A. Dubietis, "Infrared extension of femtosecond supercontinuum generated by filamentation in solid-state media," Appl. Phys. B **116**(2), 477–483 (2014).
33. P. Mackonis, A. Petrulenas, A. M. Rodin, V. Girdauskas, and A. Michailovas, "Two-stage transient stimulated Raman chirped-pulse amplification in $KGd(WO_4)_2$ with compression to 145 fs," Opt. Lett. **45**(24), 6627–6630 (2020).
34. N. Daher, X. Delen, F. Guichard, M. Hanna, and P. Georges, "Raman wavelength conversion in a multipass cell," Opt. Lett. **46**(14), 3380–3383 (2021).
35. A. Petrulenas, P. Mackonis, and A. M. Rodin, "Synthesis of adjacent Stokes spectra in a two-stage transient stimulated Raman chirped-pulse amplifier," Crystals **12**(7), 888 (2022).
36. W. Ryba-Romanowski, S. Golab, P. Solarz, G. Dominiak-Dzik, and T. Lukasiewicz, "Anti-Stokes emission in undoped YVO_4," Appl. Phys. Lett. **80**(7), 1183–1185 (2002).
37. I. A. Khodasevich, A. S. Grabtchikov, A. A. Kornienko, and E. B. Dunina, "Blue luminescence in YVO_4 and $KGd(WO_4)_2$ crystals excited by CW 1064-nm radiation," Opt. Spectrosc. **119**(5), 759–765 (2015).
38. A. Brodeur and S. L. Chin, "Band-gap dependence of the ultrafast white-light continuum," Phys. Rev. Lett. **80**(20), 4406–4409 (1998).
39. A. Dubietis, V. Jukna, and A. Couairon, *The Supercontinuum Laser Source: Supercontinuum in IR-MIR from Narrow Bandgap Bulk Solid-State Materials*, R. R. Alfano, ed. (Springer Nature Switzerland, 2022), pp. 457–477.
40. C. B. Schaffer, J. F Garcia, and E. Mazur, "Bulk heating of transparent materials using a high-repetition-rate femtosecond laser," Appl. Phys. A **76**(3), 351–354 (2003).
41. A. Marcinkevičiūtė, G. Tamošauskas, and A. Dubietis, "Supercontinuum generation in mixed thallous halides KRS-5 and KRS-6," Opt. Mater. **78**, 339–344 (2018).
42. F. Vernuccio, A. Bresci, B. Talone, A. De La Cadena, C. Ceconello, S. Mantero, C. Sobacchi, R. Vanna, G. Cerullo, and D. Polli, "Fingerprint multiplex CARS at high speed based on supercontinuum generation in bulk media and deep learning spectral denoising," Opt. Express **30**(17), 30135–30148 (2022).